

---

This is an electronic reprint of the original article.  
This reprint may differ from the original in pagination and typographic detail.

Tuononen, Ari J.; Kriston, András; Persson, Bo  
**Multiscale physics of rubber-ice friction**

*Published in:*  
Journal of Chemical Physics

*DOI:*  
[10.1063/1.4962576](https://doi.org/10.1063/1.4962576)

Published: 21/09/2016

*Document Version*  
Publisher's PDF, also known as Version of record

*Please cite the original version:*  
Tuononen, A. J., Kriston, A., & Persson, B. (2016). Multiscale physics of rubber-ice friction. *Journal of Chemical Physics*, 145(11), Article 114703. <https://doi.org/10.1063/1.4962576>

---

This material is protected by copyright and other intellectual property rights, and duplication or sale of all or part of any of the repository collections is not permitted, except that material may be duplicated by you for your research use or educational purposes in electronic or print form. You must obtain permission for any other use. Electronic or print copies may not be offered, whether for sale or otherwise to anyone who is not an authorised user.

## Multiscale physics of rubber-ice friction

Ari J. Tuononen, András Kriston, and Bo Persson

Citation: *The Journal of Chemical Physics* **145**, 114703 (2016); doi: 10.1063/1.4962576

View online: <https://doi.org/10.1063/1.4962576>

View Table of Contents: <http://aip.scitation.org/toc/jcp/145/11>

Published by the [American Institute of Physics](#)

---

### Articles you may be interested in

[Ice friction: Role of non-uniform frictional heating and ice premelting](#)

*The Journal of Chemical Physics* **143**, 224701 (2015); 10.1063/1.4936299

[Physics of ice friction](#)

*Journal of Applied Physics* **107**, 081101 (2010); 10.1063/1.3340792

[Theory of rubber friction and contact mechanics](#)

*The Journal of Chemical Physics* **115**, 3840 (2001); 10.1063/1.1388626

[Ice friction: The effects of surface roughness, structure, and hydrophobicity](#)

*Journal of Applied Physics* **106**, 024303 (2009); 10.1063/1.3173346

[General contact mechanics theory for randomly rough surfaces with application to rubber friction](#)

*The Journal of Chemical Physics* **143**, 224111 (2015); 10.1063/1.4936558

[Rubber friction on road surfaces: Experiment and theory for low sliding speeds](#)

*The Journal of Chemical Physics* **142**, 194701 (2015); 10.1063/1.4919221

---

PHYSICS TODAY

WHITEPAPERS

#### ADVANCED LIGHT CURE ADHESIVES

Take a closer look at what these environmentally friendly adhesive systems can do

READ NOW

PRESENTED BY  
 **MASTERBOND**  
ADHESIVES | SEALANTS | COATINGS

## Multiscale physics of rubber-ice friction

Ari J. Tuononen,<sup>1,a)</sup> András Kriston,<sup>2,b)</sup> and Bo Persson<sup>3</sup>

<sup>1</sup>Department of Mechanical Engineering, Aalto University, Espoo, Finland

<sup>2</sup>Goodyear SA, Colmar-Berg, Luxembourg

<sup>3</sup>PGI, FZ-Jülich, Jülich, Germany

(Received 15 June 2016; accepted 29 August 2016; published online 20 September 2016)

Ice friction plays an important role in many engineering applications, e.g., tires on icy roads, ice breaker ship motion, or winter sports equipment. Although numerous experiments have already been performed to understand the effect of various conditions on ice friction, to reveal the fundamental frictional mechanisms is still a challenging task. This study uses *in situ* white light interferometry to analyze ice surface topography during linear friction testing with a rubber slider. The method helps to provide an understanding of the link between changes in the surface topography and the friction coefficient through direct visualization and quantitative measurement of the morphologies of the ice surface at different length scales. Besides surface polishing and scratching, it was found that ice melts locally even after one sweep showing the refrozen droplets. A multi-scale rubber friction theory was also applied to study the contribution of viscoelasticity to the total friction coefficient, which showed a significant level with respect to the smoothness of the ice; furthermore, the theory also confirmed the possibility of local ice melting. *Published by AIP Publishing.* [<http://dx.doi.org/10.1063/1.4962576>]

### I. INTRODUCTION

Low grip, which often occurs on ice surfaces, is potentially dangerous. In fact, motor vehicle collisions are globally one of the leading causes of fatal accidents<sup>1</sup> and such accidents are often caused by slippery roads. The absence of a strong enough grip can be harmful for humans, not only in the case of vehicle tires but also for shoes. Globally, falls represent the third most common cause of disability and the second of fatal accidents.<sup>2</sup> The ongoing Arctic boom is definitely increasing activities in icy conditions, and thus, a better understanding is required so that people can work safely and operate machines reliably in these conditions. These risks and consequences can be reduced with a better understanding of the friction processes on icy surfaces.

Rubber friction theory has advanced greatly in the last ten years, but there is still no consistent and complete theory explaining the friction between rubber and ice. Historically, Michael Faraday was one of the first to study ice friction with an ice cube experiment, in which he showed that when brought together two ice cubes stick to each other well below the melting point of ice.<sup>3–5</sup> This was the first experiment to indicate that water molecules on ice surfaces may have higher mobility than in bulk ice, as if the ice surface were covered by a thin liquid-like (premelted) layer of water molecules. However, from 1850, for many decades the low friction observed on ice was usually explained as resulting from pressure melting of ice, until 1939, when Bowden and Hughes<sup>6</sup> proposed that frictional heating explains the slipperiness of ice.

Understanding of the interplay between the multi-scale roughness of real surfaces and the multi-frequency viscoelastic response function of rubber initiated the progress in rubber

friction research.<sup>7,8</sup> In these theories, the hysteresis energy loss of rubber in cyclic deformation, in response to the perturbing deformations of the rubber caused by the asperities of the road, was no longer just a qualitative way of explaining rubber friction (as in Ref. 9), but there was a first-principle theory predicting the viscoelastic contribution to the friction coefficient  $\mu$ . If an ice surface exhibits enough surface roughness, the viscoelastic deformations of the rubber can produce a significant friction force even for temperatures close to the melting point of ice, see Fig. 1.

It is unclear that to what extent an ice surface actually melts when an obstacle slides on it, and a multiscale approach is necessary in order to understand this problem better. The melting could be caused by the high local pressure in asperity contact regions or result from local frictional heating. It is possible that melting modifies only the short wavelength roughness on the top of larger asperities that can still contribute to viscoelastic friction (see Fig. 1). Also, even if melting is observed on the ice surface after an obstacle has been sliding on it, one cannot conclude that melting is responsible for the reduction in  $\mu$ , because melting may occur only near the trailing edge of the slider, and thus most of the contact would be dry.

Pressure melting is believed not to contribute to ice friction. However, demonstrative calculations are often based on the apparent contact area to estimate the contact pressure, but in most cases the real contact area is only of the order  $\sim 1\%$  of the apparent contact area. Thus, the actual (high) local contact pressure could affect ice friction by pressure melting as well. However, in most cases the ice will yield plastically before the pressure becomes high enough to result in pressure melting. In fact, the penetration hardness of ice is rather low (of the order  $\sim 10\text{--}100$  MPa depending on the temperature and the indentation speed), i.e., below the pressure needed for pressure melting except when the temperature is very close to

<sup>a)</sup>Electronic mail: ari.tuononen@aalto.fi

<sup>b)</sup>Also at Department of Mechanical Engineering, Aalto University, Finland.

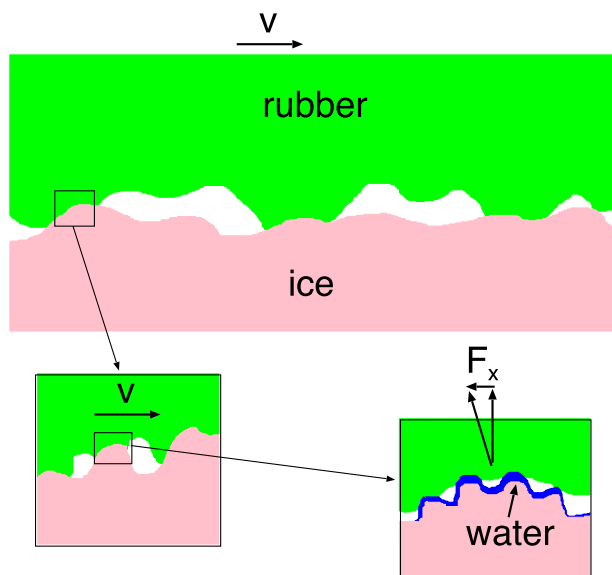


FIG. 1. Multiscale rubber-ice contact. At the highest magnification  $\zeta_1$  it is observed that the ice-rubber contact regions are separated by a thin film of water which reduces the contribution to the friction from the area of contact. However, there may still be a large contribution to the friction force from the viscoelastic deformations of the rubber from the roughness observed at lower magnification  $\zeta < \zeta_1$  (i.e., the more long-wavelength roughness) since this roughness is unaffected by the ice melting.

the melting temperature of ice. In addition, rubber is a rather soft material and thus the conditions for pressure melting are not favorable.

There are many experimental studies using pin-on-disk type devices. In this methodology, the slider moves on the ice surface repeatedly until the sliding friction coefficient stabilizes. It is difficult to imagine any application where the obstacle goes over the same ice surface repeatedly. Thus, we think that it is more interesting to study the evolution of friction and surface topography as a function of the number of sliding sweeps over the same ice surface. This approach can also be used to explain why virgin ice is not necessarily slippery.

In this paper, we present a unique *in situ* ice topography measurement (white light interferometer (WLI), cold chamber installation) that reveals the length scale at which ice actually melts. We also calculate the contribution to the ice-rubber friction from rubber viscoelastic deformations induced by the ice surface roughness, and we estimate the temperature increase in the rubber-ice contact regions and determine under which conditions ice melting is likely to occur.

## II. MULTISCALE ICE SURFACE EVOLUTION UNDER RUBBER SLIDER

The friction tests were performed with an in-house linear friction tester (Figure 2), optimized for ice friction testing.<sup>10</sup> The linear friction tester was in a climate chamber with massive wall insulation providing a stable environment for the testing. The climate chamber was temperature controlled ( $T = -5^\circ\text{C}$ ) and the temperature probe was located near the ice surface. The friction forces include the inertia of the

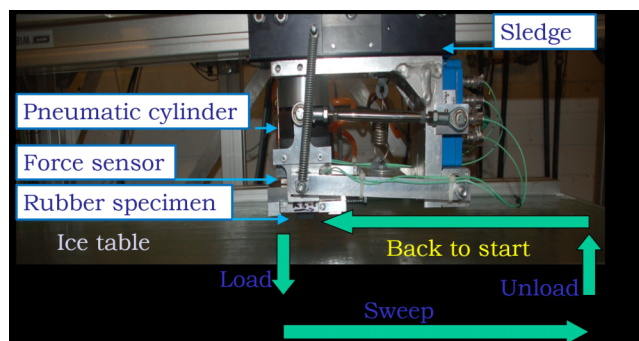


FIG. 2. Linear friction tester.

slider, but its influence on the results is negligible. The test surface was a  $15 \times 30$  cm glass plate with ice on top of it. The ice surface was built up layer by layer using distilled water and flooding technique until final ice thickness of 2 mm was reached. This ice plate had a socket both in the linear friction tester and white light interferometer (Bruker Contour GT-K Automated System). Thus, the ice topography could be measured easily and quickly during ongoing ice friction testing. The linear friction tester and WLI were both in the same cold chamber and roughly 1.5 m apart. The operator had to cover their entire skin so as not to expose the ice surface to any heat. Three different objectives (5 $\times$ , 10 $\times$ , and 50 $\times$ ) were used to map a large range of length scales. Image stitching was used to get topographies with a high resolution covering a wide macroscopic area. The length scale range obtainable with this methodology was from 98 nm (pixel size) to 5 mm (the largest area measured). The profilometer measurement color was narrowband green (limits practical lateral resolution) as it gave the fewest outliers in the measurements.

Figure 3 shows the ice surface topography for different numbers of sweeps (passings over the same ice surface area) and for different magnifications (different WLI objectives). The images show grain boundaries at all length scales, but the scratches appearing in the sliding direction are more visible at low magnification, whereas small droplet-like features are observed only in the images with the highest magnification. Scratches appear mainly over 10  $\mu\text{m}$  and are thus slightly smaller features than the typical width of a grain boundary. The scratches are probably caused by filler agglomerates<sup>11</sup> on the rubber surface that touch the ice surface.

The images with the lowest magnification (area 5 mm  $\times$  5 mm) show that the number of scratches increases, and also that the grain boundaries on the surface become less visible (this partly depends on the scaling of the color bar) with an increasing number of sweeps. Note that at this magnification, it appears that the rubber is in contact with the ice everywhere, i.e., also at the bottom of the deepest long-wavelength valleys in the ice surface. However, the scratches on the top of the asperities are deeper than those in the valleys (Fig. 4), indicating higher local contact pressure on the top of the asperities. As a result, a peak asperity in the middle of the topography nearly disappears after 50 sweeps. With an increasing number of sweeps, the original topography diminishes and is replaced by scratches in the

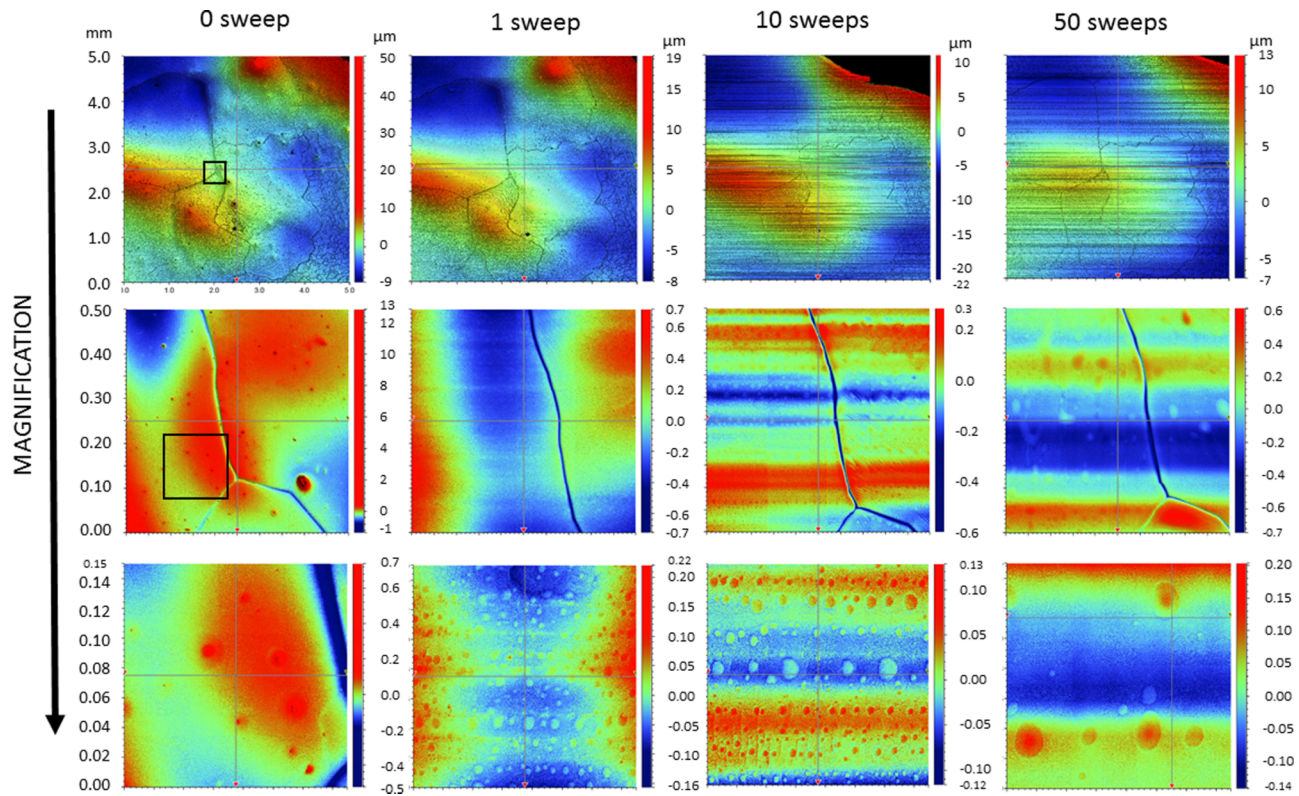


FIG. 3. Multiscale topography of ice surface as a function of the number of sweeps (velocity 0.5 m/s, pressure 0.24 MPa, and temperature  $-5^{\circ}\text{C}$ ). All images were focused near the triple join of grain boundaries in the center of image. A black box indicates image location for the next magnification level (shown for 0 sweep case).

sliding direction. It is very likely that the fine scratches are caused by silica filler particles ( $<100\text{ nm}$ ). No melting can be observed at this length scale.

Let us estimate the contribution to the friction from the scratching (plowing) of the ice surface by the rubber filler particles (see Figs. 3 and 4). The rubber block used in the experiments has a nominal contact area with the ice  $A_0 = L \times L$  with  $L = 2.5\text{ cm}$ . In an experiment performed

at the nominal contact pressure  $p = F_N/A_0 \approx 0.2\text{ MPa}$ , we observe on average  $N \approx 35$  scratches with an average width  $\Delta y \approx 23\ \mu\text{m}$  and depth  $\Delta z \approx 0.25\ \mu\text{m}$  and cross-sectional area  $A_c \approx \Delta y \Delta z / 2 \approx 3\ \mu\text{m}^2$ . We assume that the effective ice penetration hardness is  $\sigma_Y \approx 5\text{ MPa}$  (see Refs. 12–14). The force required to scratch the ice is approximately given by  $F \approx N A_c \sigma_Y$ . Using the information above, the contribution to the friction coefficient from scratching (plowing) can

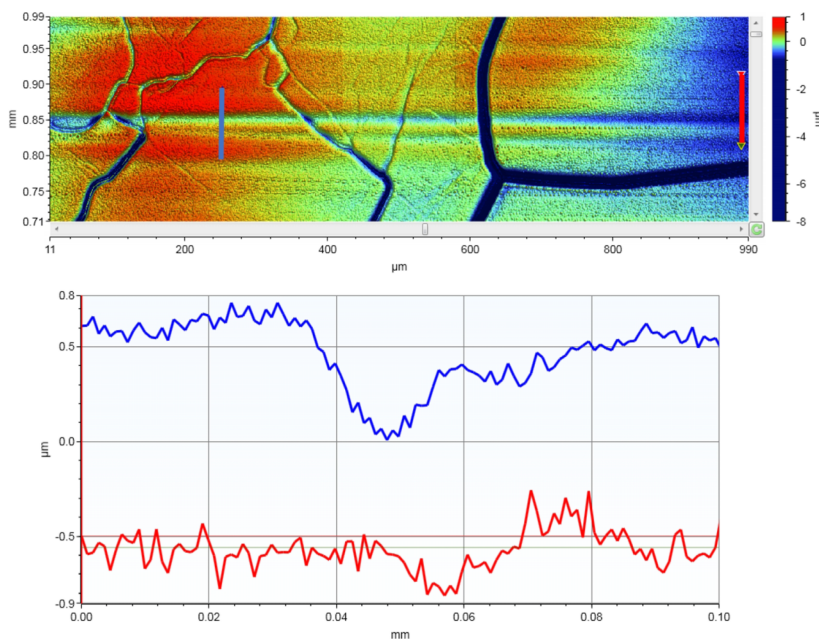


FIG. 4. Scratch dimensions. The blue line shows the topography on the top of the asperity and the red line that in the valley.

be calculated to be  $\Delta\mu = F/F_N \approx 4 \times 10^{-6}$ , i.e., completely negligible.

The middle magnification (area  $0.5 \text{ mm} \times 0.5 \text{ mm}$ ) shows that grain boundaries appear as a negative feature on the surface. Positive features (possibly debris or loosely bound asperities) are easily swept away and probably will not contribute to the friction, even though they have an influence on the surface roughness power spectrum at short length scales (see Fig. 9). The same grain boundary can be seen even after 50 sweeps, when all the other features on the surface have been swept away. Round features which might be frozen meltwater droplets appear on the surface after 50 sweeps.

The images with the highest magnification (area  $0.15 \text{ mm} \times 0.15 \text{ mm}$ ) that we can access by the optical non-contact method show important features on the ice surface which might be interpreted as noise if only based on images with a lower magnification. Before sliding, a very sharp edge of a grain boundary is seen (depth  $400 \text{ nm}$ ). Even after one sweep, circular positive features appear on the surface, and they are probably frozen meltwater droplets on the surface. The lateral size of a typical droplet is around  $5\text{--}10 \mu\text{m}$  and the typical height is  $10\text{--}50 \text{ nm}$ . Thus, the droplets are very flat as a result of the high wettability of ice, and also the dimensions and shape generally agree with the  $\alpha$ -phase liquid-like droplets observed by Sazaki.<sup>15</sup> However, in our case the droplets are not randomly distributed, but they appear as lines aligned in the sliding direction. Thus, the roughness at the trailing edge of the sample channels water into these sequences of droplets. It is a significant result that the droplets exist both on the peaks and in the valleys; thus, they are not flowing into the valleys, which indicates that the meltwater freezes rather quickly, or is only in a quasi-liquid state (e.g., a highly viscous fluid-like state as proposed in Refs. 16 and 17). The number of droplets does not increase with the number of sweeps. Actually, the number of droplets decreases significantly for the 50-sweep topography, but the size of the droplets increases, which indicates that smaller droplets merge into larger droplets. No “sausage-shaped” meltwater features<sup>18</sup> were observed and it is possible that they only form in a pin-on-disk device where continuous sweeps spread individual droplets onto these ridges.

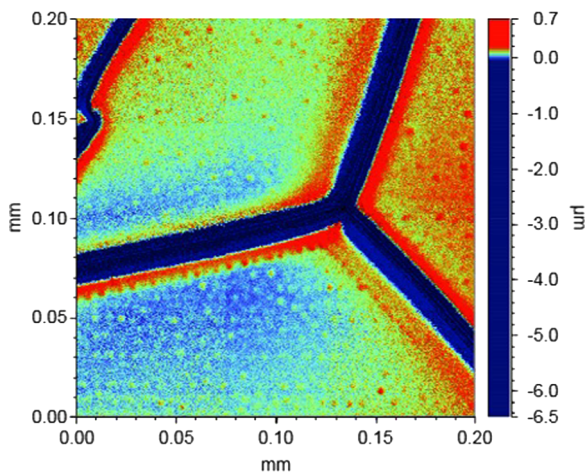


FIG. 5. Droplets near grain boundaries after one sweep over the ice surface.

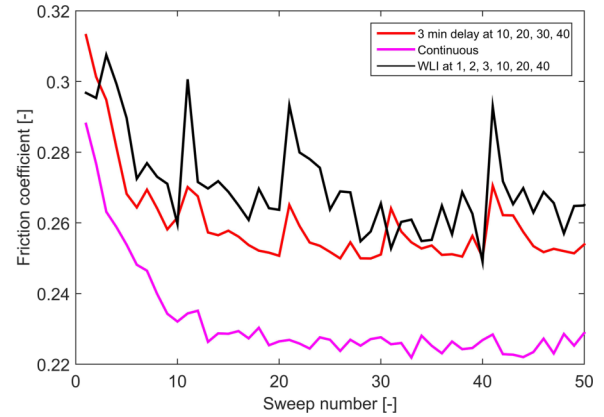


FIG. 6. Effect of WLI and waiting time on friction coefficient evolution. The continuous sweeping case is given as a comparison.

The droplets seen in Fig. 3 (1 sweep,  $150 \mu\text{m}$  range) and Fig. 5 may originate from melted virgin ice asperities (0 sweeps image) and/or from a liquid-like layer of premelted ice which may become more liquid-like as a result of the frictional heating of the ice surface. Indeed, Engemann proposed that the density of the quasi-liquid-like state approaches density of water near its melting temperature.<sup>19</sup> The droplets cover roughly 22% of the area and their average area is  $31 \mu\text{m}^2$  and their height  $31 \text{ nm}$ . Thus, the frozen droplets are very flat. If the volume of the droplets were to be distributed as a smooth water layer, the thickness would be around  $4 \text{ nm}$ . This would match the estimated thickness of the quasi-liquid-like layer in Refs. 15 and 17.

The evolution of the friction coefficient  $\mu$  as a function of sweeps is shown in Fig. 6. It can be observed that WLI measurement that takes 3-5 min has a similar influence on  $\mu$  to that of the waiting time. Thus, it is believed that the optical topography measurement itself has no significant effect on the results. However, when the sweeping is performed continuously, the evolution of  $\mu$  is smoother. All cases indicate that  $\mu$  converges to a stable value after 10 sweeps, and the friction is always at its highest for one of the first sweeps. It was observed in Ref. 20 that the increment in  $\mu$  resulting from the waiting time originates from the ice cooling more than the rubber cooling towards the ambient temperature.

### III. ICE SURFACE ROUGHNESS ANISOTROPY AND POWER SPECTRUM

The optical pictures presented above give a qualitative insight into important processes occurring on different length scales during the sliding of a rubber block on an ice surface. Rubber friction and other contact mechanics quantities require quantitative information about the roughness on all (relevant) length scales. In the contact mechanics theory of Persson, all the necessary information about the surface roughness is contained in the two-dimensional (2D) surface roughness power spectrum defined by<sup>7,21</sup>

$$C(\mathbf{q}) = \frac{1}{(2\pi)^2} \int d^2x \langle h(\mathbf{x})h(\mathbf{0}) \rangle e^{i\mathbf{q}\cdot\mathbf{x}}, \quad (1)$$

where  $h(\mathbf{x})$  is the surface height at point  $\mathbf{x} = (x, y)$ , and where  $\langle \dots \rangle$  stands for ensemble averaging. It is assumed that  $\langle h(\mathbf{x}) \rangle = 0$ . For a surface with isotropic roughness, the power spectrum  $C(\mathbf{q})$  depends only on the magnitude  $q = |\mathbf{q}|$  of the wavevector. The ice surfaces we use have anisotropic roughness after sliding. The anisotropy of surface roughness can be characterized by the Peklenik and Tripp numbers. Roughly speaking, the Peklenik and Tripp numbers are the ratio  $\gamma = \xi_x/\xi_y$  between the axis of the elliptic cross section (in the  $xy$ -plane) of an (average) asperity in real  $(x, y)$  space and in wavevector  $(q_x, q_y)$  space, respectively. Clearly, for 1D roughness,  $\gamma = \infty$  or  $0$  if the  $x$ -axis is along or orthogonal to the “roughness lines,” while for isotropic roughness  $\gamma = 1$ . The Tripp number is most important in practical applications, e.g., it appears in the equations which determine the fluid flow at the interface between two solids. Since roughness appears differently at different length scales, the Tripp number depends on the wavenumber  $q$  (or wavelength  $\lambda = 2\pi/q$ ),  $\gamma = \gamma(q)$ . The Tripp number can be easily obtained from the 2D surface roughness power spectrum  $C(\mathbf{q})$  using<sup>22</sup>

$$\gamma = \frac{1}{2|D|} \left[ 1 - (1 - 4|D|)^{1/2} \right] - 1, \quad (2)$$

where  $|D|$  is the determinant of the tensor,

$$D(q) = \frac{\int_0^{2\pi} d\phi C(\mathbf{q})\mathbf{q}\mathbf{q}/q^2}{\int_0^{2\pi} d\phi C(\mathbf{q})}, \quad (3)$$

where  $\mathbf{q} = q(\cos \phi, \sin \phi)$ .

To expand on this definition, note that  $D_{11} + D_{22} = \text{Tr}D = 1$  and that the  $D$  is symmetric and can be diagonalized. We denote the diagonal elements as  $D_{11} = 1/(1 + \gamma)$  and  $D_{22} = \gamma/(1 + \gamma)$ . Note that  $|D| = D_{11}D_{22} = \gamma/(1 + \gamma)^2$ . This equation has the solution  $\gamma$  given by (2). Note that the definition (2) of  $\gamma$  is independent of the coordinate system used since the determinant is invariant under rotations (orthogonal transformations). Note also that for a surface with isotropic statistical properties, we get  $D_{ij} = \delta_{ij}/2$  so that  $|D| = 1/4$  and from (2)  $\gamma = 1$  as it should. In Fig. 7 we show the Tripp surface asymmetry number  $\gamma$  as a function of the logarithm of the wavenumber  $q$  for different numbers of sweeps.

Figure 8 shows the (angular averaged) surface roughness power spectrum of the virgin ice and rubber. It can be seen that the rubber surface is rougher than the ice surface, and thus, in this case the contact mechanics differ significantly from those of rubber in contact with, e.g., concrete, even without any frictional melting, as it was shown in Ref. 23 where contact area analysis was performed between a worn rubber sample and flat countersurface. Consequently, in the calculations below, we use an extension of the original friction model<sup>7</sup> which includes the slider roughness.<sup>24</sup>

Figure 9 shows the one-dimensional (1D) power spectrum of the ice surface in the sliding direction ( $x$ -direction) and in the  $y$ -direction before sliding and after one, 10, and 50 sweeps. Interestingly, even the first sweep modifies the ice surface significantly, which may be explained by the removal of loose asperities and dust on the virgin ice surface. As the number of sweeps increases, the power spectrum in the sliding

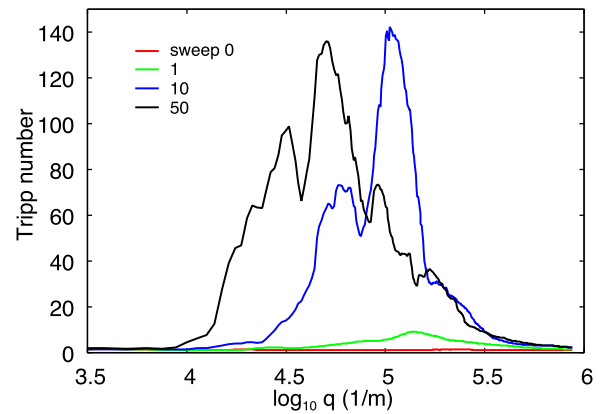


FIG. 7. The Tripp surface asymmetry number  $\gamma$  as a function of the logarithm of the wavenumber  $q$  for different numbers of sweeps. For isotropic roughness  $\gamma = 1$ , while  $\gamma > 1$  and  $\gamma < 1$  depending on whether the roughness is elongated in the  $x$  or  $y$ -direction, respectively. The original ice surface (0 sweeps) has, as expected,  $\gamma \approx 1$ , i.e., it has isotropic roughness, while the magnitude of  $\gamma$  increases and the maximum of  $\gamma(q)$  shifts to smaller wavenumbers (i.e., longer wavelength  $\lambda = 2\pi/q$ ) as the number of sweeps increases. This is exactly what is expected since when the number of sweeps increases the average wavelength (in the  $y$ -direction orthogonal to the sliding direction) of the roughness introduced by the scratching by the filler particles will increase. This is similar to, e.g., when an originally perfectly flat surface is sandblasted, where the long-wavelength roll-off of the power spectrum moves to a longer wavelength as the duration of the sandblasting increases.<sup>38</sup>

direction ( $x$ -direction) hardly changes at all (also Fig. 10), while it increases in the  $y$ -direction which can be explained by the scratches. Note also that the region where the power spectrum increases shifts to a smaller wavenumber (i.e., to a longer wavelength) as the number of sweeps increases. This is similar to what was observed for the Tripp number (see Fig. 7) and is expected from the theory. The fact that the power spectrum does not decrease significantly after the first sweep indicates that the reduction in  $\mu$  between one and 10 sweeps is due to an increase in the ice temperature and not, e.g., to the polishing of the ice surface. The power spectrum at the shortest wavevectors  $\sim 10^3 \text{ m}^{-1}$  (corresponding to a wavelength  $\lambda$  of order a few mm) is dominated by the size of the

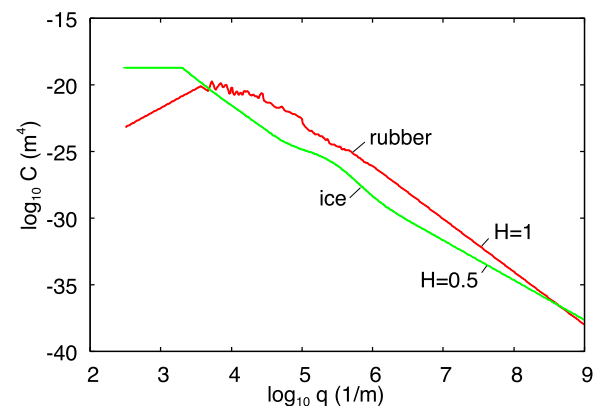


FIG. 8. The surface roughness power spectrum of the ice surface (green) and of the rubber surface (red) as a function of the wavenumber  $q$  ( $\log_{10}$ - $\log_{10}$  scale). The power spectra for  $q < 10^6 \text{ m}^{-1}$  were obtained from the surface topography measured using an optical method. The power spectrum for  $q > 10^6 \text{ m}^{-1}$  was obtained by linear extrapolation.

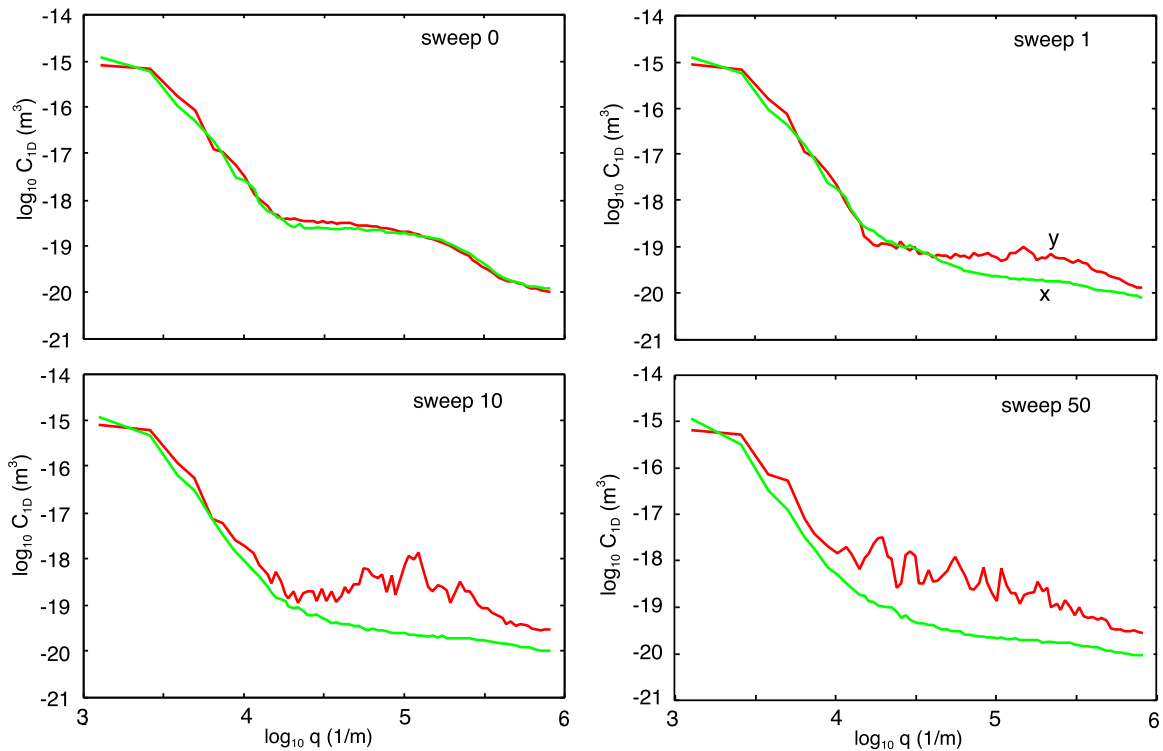


FIG. 9. The 1D surface roughness power spectra in the  $x$  and  $y$ -directions for the ice surface after zero, one, 10, and 50 sweeps. Including the roughness in the studied wavelength region, all the surfaces have an rms-roughness amplitude of  $2.2 \pm 0.2 \mu\text{m}$  while an rms-slope in the  $x$ -direction: 0.076, 0.054, 0.056, and 0.055, respectively, and in the  $y$ -direction: 0.076, 0.077, 0.11, and 0.103, respectively.

grains, and the increase in the power spectrum after  $\sim 10^5 \text{ m}^{-1}$  ( $\lambda \sim 20\text{--}60 \mu\text{m}$ ) is due to the width of the grain boundaries. Unfortunately, grain boundaries are deep valleys that lift the power spectrum, but they cannot contribute significantly to the viscoelastic dissipation which is favorable for rubber sliding friction.

#### IV. VISCOELASTIC CONTRIBUTION TO RUBBER FRICTION ON ICE

When a rubber block is sliding on an ice surface, friction will result from two processes, namely, (a) the viscoelastic deformation of the rubber resulting from interactions with ice

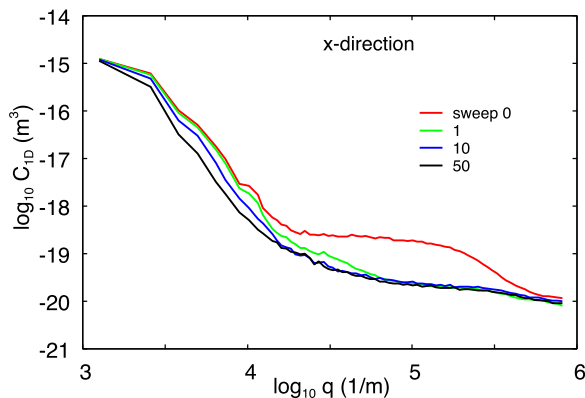


FIG. 10. The 1D surface roughness power spectra in the  $x$ -direction, i.e., in the sliding direction. For the ice surface after 0, 1, 10, and 50 sweeps.

asperities<sup>7,8</sup> and (b) the shearing of the area of real contact.<sup>25</sup> At a high enough sliding speed, frictional heating results in a thin film of water in the area of contact<sup>26,27</sup> and (b) results from the shearing of this film (frictional shear stress  $\tau_f \approx \eta v/h$ , where  $h$  is the thickness of film of water and  $\eta$  the viscosity of the water). If no meltwater film is produced, the frictional shear stress  $\tau_f$  may instead result from the adhesive interaction between the ice surface and the rubber molecules at the sliding interface<sup>28</sup> or from the shearing of a viscous premelted film.<sup>17,29</sup>

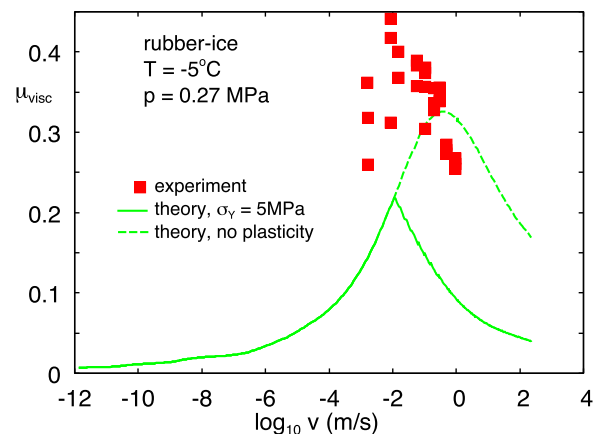


FIG. 11. The measured (red squares) and the calculated (green line) friction coefficients for the temperature  $T = -5^\circ\text{C}$  and the nominal contact pressure  $p = 0.27 \text{ MPa}$ . The dashed green line is the result using the power spectra in Fig. 8 but with the cutoff wavenumber  $q_1$  determined by the ice penetration hardness  $\sigma_Y$  (see text for details).

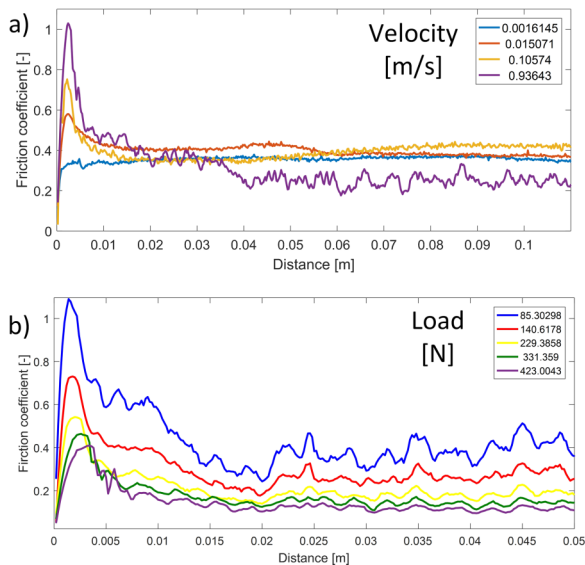


FIG. 12. (a) Friction coefficient as a function of sliding distance for different velocities [m/s] at  $-5^{\circ}\text{C}$ . The nominal contact area of the sample is  $25 \times 25$  mm and the load is 200 N. (b) Friction coefficient as a function of sliding distance for different vertical loads (in Newton) at  $-5^{\circ}\text{C}$ . The nominal contact area of the sample is  $25 \times 25$  mm and the velocity is  $v = 0.5$  m/s. In each case the dwell time equals 2 s.

Let us first study the viscoelastic contribution to the friction, assuming there is no or negligible smoothing of the ice surface resulting from the melting of the ice surface (e.g., the condition at the leading edge of a slider). The ice surfaces we have used are relatively smooth, and even if we include (by linear extrapolation as shown in Fig. 8) all the roughness down to a wavelength of a few nanometers, corresponding to the large wavenumber cutoff  $q_1 \approx 10^9 \text{ m}^{-1}$ , the theoretically predicted friction is rather small, see Fig. 11, but rather close to what is observed experimentally during steady sliding, where a thin film of water is likely to exist in the rubber-ice contact regions.

Fig. 12 shows the measured friction coefficient as a function of the sliding distance for several sliding speeds and several loads. It is interesting to note that the friction typically exhibits a relatively large peak at small sliding distances of the order of  $s = 1\text{--}3$  mm. We will now argue that this peak is, at least in part, related to frictional heating and the softening or melting of the ice in the asperity contact regions, which require a slip distance of a few millimeters to occur.

## V. FRICTIONAL HEATING AND SURFACE MELTING OF ICE

We calculated the temperature in the rubber-ice contact regions using the theory presented in Ref. 30. The ice and rubber roughness power spectra were included into the theory and Dynamic Mechanical Analysis (DMA) was completed for the rubber compound (see the Appendix). In the calculations we only include the viscoelastic contribution to the friction, but below we will discuss how the results are modified when the frictional heating resulting from the dissipative processes in the area of real contact is included in the analysis.

Fig. 13(a) shows the calculated temperature in the ice-rubber asperity contact regions as a function of sliding speed for several sliding distances  $s = 0.1, 0.25, 0.5,$  and  $1$  cm. The temperature at the start of the sliding equals  $T = T_0 = -5^{\circ}\text{C}$  everywhere, and the nominal contact pressure  $p = 0.27$  MPa. The calculation only includes the viscoelastic contribution to the friction (dashed line in Fig. 11), and the actual temperature increase before the melting of the ice occurs will be larger (by a factor  $\sim 2\text{--}3$ ) than the calculated values as a result of the contribution to frictional heating of the shearing of the area of real contact. In Fig. 12 at the lowest sliding speed  $v \approx 0.16$  cm/s, no peak is observed, indicating that the melting of the ice does not take place at this sliding speed. This is consistent with the results in Fig. 13(a), where the temperature increase for that velocity is negligible for all the sliding distances under consideration.

For the sliding speed  $v \approx 1.5$  cm/s, a small peak is observed (Fig. 12) but no ice melting for short sliding distances is expected in this case either. However, taking into account the fact that the experimental friction coefficient is about twice as large as the viscoelastic contribution (about 0.5 instead of the viscoelastic contribution, which is of the order of 0.25 for this sliding speed according to Fig. 11), the temperature increase is about double than that given in Fig. 13(a), i.e.,

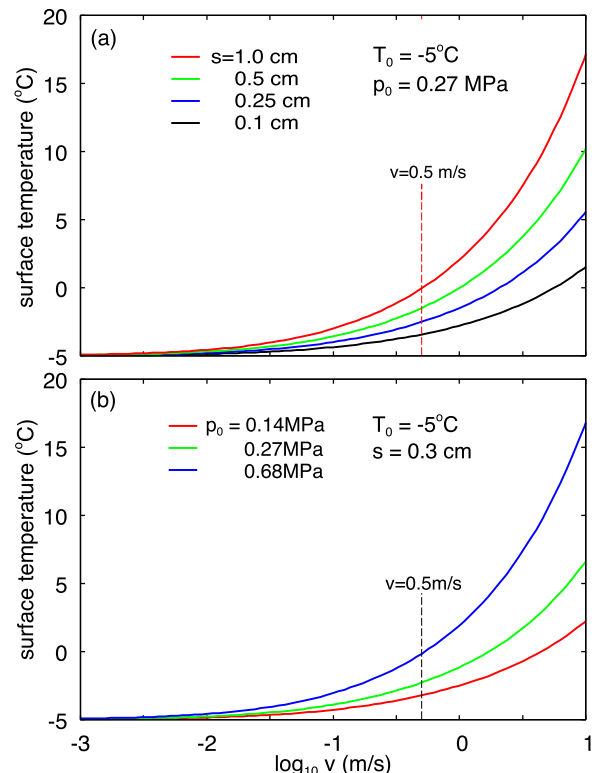


FIG. 13. The calculated temperature in the ice-rubber asperity contact regions as a function of (a) sliding speed for several sliding distances  $s = 0.1, 0.25, 0.5,$  and  $1$  cm and (b) for several nominal contact pressures  $p_0 = 0.14, 0.27,$  and  $0.68$  MPa. The temperature at the start of the sliding equals  $T = T_0 = -5^{\circ}\text{C}$  everywhere, and in (a) the nominal contact pressure  $p = 0.27$  MPa and in (b) the sliding distances  $s = 0.3$  cm. The calculation only includes the viscoelastic contribution to the friction (dashed line in Fig. 11), and the actual temperature increase before melting of ice occurs will be larger than the calculated values due to the contribution to frictional heating from shearing the area of real contact.

of the order of 1 or 2 °C depending on the sliding distance. This temperature increase could soften the ice surface<sup>29</sup> and result in a reduction in the frictional shear stress which would contribute to the peak observed at short sliding distances. In addition, there may be an increased friction at the start-up of the sliding resulting from an increase in the area of real contact during the time of stationary contact (dwell time 2 s) as a result of thermally activated creep processes.<sup>31–34</sup> Similar physical processes may explain the peak in the friction observed for the sliding speed  $v \approx 0.11$  m/s. Finally, for the highest sliding speed  $v \approx 0.94$  m/s, the melting of the ice will already take place after a sliding distance of the order of 1 mm. Here we have taken into account the fact that the friction coefficient before the melting of the ice surface is very high, of the order of unity (see Fig. 12), which will result in a temperature increase which is about three times bigger than indicated in Fig. 13(a), which only includes the viscoelastic contribution to the friction coefficient.

Let us now discuss the dependency of the friction coefficient on the sliding distance as we change the normal force or load. Fig. 13(b) shows the calculated temperature in the ice-rubber asperity contact regions as a function of the sliding speed for several nominal contact pressures  $p_0 = 0.14$ , 0.27, and 0.68 MPa. The temperature at the start of the sliding equals  $T = T_0 = -5$  °C everywhere, and the sliding distances  $s = 0.3$  cm. The calculation only includes the viscoelastic contribution to the friction (dashed line in Fig. 11), and the actual temperature increase before the melting of the ice occurs will be larger than the calculated values (by a factor  $\sim 2$ – $3$ ) as a result of the contribution to frictional heating of the shearing of the area of real contact.

The experimental data shown in Fig. 12 were obtained for the sliding speed  $v = 0.5$  m/s, as indicated by the vertical dashed line in Fig. 13(b). Note that there is a direct correlation between the calculated frictional heating and the heights of the peaks in Fig. 12. For the highest load, the calculated surface temperature after a sliding distance of 0.3 cm is about  $T = 0$  °C and since in reality the friction at the peak maximum in Fig. 12 is larger than the viscoelastic contribution we conclude that the ice will melt. For the lowest load the peak maximum is of the order of  $\mu \approx 1$ , i.e., about three times higher than that used in the calculation of the theory, and we conclude from Fig. 13(b) that in this case too the ice surface will melt. During steady sliding the friction coefficient decreases with an increasing load, which may arise from the same effect as discussed in Ref. 12 or may be related to the smoothing of the ice surface by the melting of the ice, which is at its greatest at the highest load.

Finally, note that in the present case, because of the relative low surface roughness, the macroasperity contact regions occupy a large fraction of the nominal contact area and in this case the following simple approximate treatment gives a useful estimate of the ice surface temperature. Assume that the surfaces are perfectly smooth and the rubber makes contact with the ice surface everywhere. Assume that the heat current  $J_0$  flows from the interface into the rubber and  $J_1$  into the ice, and that at time  $t = 0$  the temperature is  $T_0$  everywhere. In this case the rubber surface temperature at time  $t$  is given by the standard result,

$$T = T_0 + J_0 \left( \frac{4}{\pi} \frac{t}{\rho_0 C_0 \kappa_0} \right)^{1/2}, \quad (4)$$

where  $\rho_0$ ,  $C_0$ , and  $\kappa_0$  are the density, heat capacity, and thermal conductivity of the rubber. A similar equation gives the ice surface temperature. Assuming that the temperature is continuous at the rubber-ice interface, and that the total heat current  $J = J_0 + J_1 = \mu p_0 v$ , where  $v$  is the sliding speed, one can derive the interface temperature,

$$T = T_0 + \frac{\mu p_0 \sqrt{(4vs/\pi)}}{\sqrt{(\rho_0 C_0 \kappa_0)} + \sqrt{(\rho_1 C_1 \kappa_1)}}, \quad (5)$$

where  $s = vt$  is the sliding distance. This result assumes that the sliding distance  $s$  is much smaller than the width of the nominal contact region in the sliding direction. Eq. (5) predicts a temperature increase which depends on the sliding speed and pressure in a similar way as in the more exact treatment used above. But numerically the temperature increase is only about half of what we found above, which we attribute to the fact that the actual contact area between the rubber and the ice is not complete, which results in a weaker heat transfer from the rubber to the ice than that predicted by the simple treatment (5).

## VI. CONCLUSIONS

In this study we have used a multiscale approach to gain an insight into the processes which occur on different length scales when a rubber block is slid on an ice surface. Using an optical *in situ* topography measurement, we have shown that the hard filler particles on the rubber surface scratch the ice surface and strongly modify the surface topography observed at low magnification. At high magnification we observe small circular structures that are formed on the ice surface during the sliding of the rubber block, which we attribute to the rapid freezing of meltwater produced as a result of frictional heating of the rubber-ice interface. We have analyzed the experimental data using the Persson contact mechanics and rubber friction theory. It was found that the viscoelastic dissipation of automotive tread rubber compound sliding over tiny ice surface asperities makes a significant contribution to the sliding friction of virgin ice at a velocity range of 0.001–1 m/s. The calculations, supported by experiments, show that a very short sliding distance can alter high friction ice into a slippery type. This might be potentially exploited in improving the rubber grip in rolling contact applications by shortening the sliding contact area. However, the transition from static sliding also depends on the process of detachment<sup>33,35</sup> and velocity strengthening of friction has also been observed for dry contacts.<sup>36</sup>

## ACKNOWLEDGMENTS

This work was supported by a grant from the Academy of Finland (Grant No. 274516), by the Fonds National de la Recherche Luxembourg (Under Contract No. 4817172), and a joint project between Aalto University and Goodyear SA. The authors would like to thank Dr. Boris Lorenz for the DMA measurements.

## APPENDIX: RUBBER FRICTION MODEL

For dry surfaces there are two contributions to rubber friction, one from the area of real contact and one from the pulsating deformations of the rubber surface resulting from the substrate asperities. The latter contribution depends on the internal friction of the rubber. We will assume that the friction force can be written as the sum of the viscoelastic contribution  $F_{\text{visc}}$  and a contribution from the area of real contact, which we assume is proportional to the contact area  $A$ ,

$$F_f = F_{\text{visc}} + \tau_f A, \quad (\text{A1})$$

where  $\tau_f$  is the frictional shear stress acting in the area of contact. If we write the normal force as  $F_N = p_0 A_0$ , where  $p_0$  is the nominal contact pressure and  $A_0$  the nominal contact area, we get

$$\mu = \mu_{\text{visc}} + \frac{\tau_f}{p_0} \frac{A}{A_0}. \quad (\text{A2})$$

In the present study, we will assume that a thin meltwater film separates the sliding surfaces in the area of real contact. In this case, even if the thickness of the film of water is only a few nm, the contribution to the friction from the area of contact is very small and we will neglect it in the present study.

Here we briefly review the Persson contact mechanics theory, which we used to calculate the area of real contact and the viscoelastic contribution to rubber friction. We consider the simplest case of sliding at a constant speed and at such a low speed that frictional heating can be neglected.

In the theory of Persson, the friction force acting on a rubber block squeezed with the stress  $p_0$  against a hard randomly rough surface is given by<sup>24,29,39</sup>

$$\begin{aligned} \mu_{\text{visc}} \approx & \frac{1}{2} \int_{q_0}^{q_1} dq q^3 C(q) S(q) P(q) \\ & \times \int_0^{2\pi} d\phi \cos \phi \operatorname{Im} \frac{E(qv(t) \cos \phi, T_0)}{(1 - \nu^2)p_0}, \end{aligned} \quad (\text{A3})$$

where  $T_0$  denotes the temperature,  $q_1$  and  $q_0$  are the large and low wave vector cutoff,  $\phi$  gives the direction of the wave vector according to the sliding direction and where

$$P(q) = \frac{1}{\sqrt{\pi}} \int_0^{\sqrt{G}} dx e^{-x^2/4} = \operatorname{erf} \left( \frac{1}{2\sqrt{G}} \right), \quad (\text{A4})$$

where

$$G(q) = \frac{1}{8} \int_{q_0}^q dq q^3 C(q) \int_0^{2\pi} d\phi \left| \frac{E(qv \cos \phi, T_0)}{(1 - \nu^2)p_0} \right|^2. \quad (\text{A5})$$

Note that  $P(q) = A(q)/A_0$  is the (normalized) contact area observed at the magnification  $\zeta = q/q_0$ .

The factor  $S(q)$  in (A3) is a correction factor which takes into account the fact that the asperity-induced deformations of the rubber are smaller than in the case in which complete contact occurred in the (apparent) contact areas observed at the magnification  $\zeta = q/q_0$ . For contact between elastic solids this factor reduces the elastic asperity-induced deformation energy, and including this factor gives a distribution of interfacial separation in good agreement with experiments and exact numerical studies. The interfacial separation describes how an elastic (or viscoelastic) solid deforms and penetrates into

the roughness valleys, and it is stressed here that these (time-dependent) deformations cause the viscoelastic contribution to rubber friction. We assume that the same  $S(q)$  reduction factor as that found for elastic contact is also valid for sliding contact involving viscoelastic solids. For elastic solids it has been found that  $S(q)$  is well approximated by

$$S(q) = \gamma + (1 - \gamma)P^2(q), \quad (\text{A6})$$

where  $\gamma \approx 1/2$ , and here we use the same expression for viscoelastic solids, being a geometrical parameter in its nature. Note that  $S \rightarrow 1$  as  $P \rightarrow 1$  which is an exact result for complete contact. In fact, for complete contact the expression (A3) is exact.

In the theory of rubber friction, the viscoelastic contribution to the friction depends on the surface roughness power spectrum  $C(q)$ , where  $q = 2\pi/\lambda$  is the wavenumber of a particular frequency component (with the wavelength  $\lambda$ ) of the roughness profile. Most surfaces have a self-affine fractal like topography, where  $C(q) \sim q^{-2(1+H)}$ . Here the Hurst exponent is typically in the range  $0.7 < H < 1$ , corresponding to a fractal dimension  $D_f = 3 - H$  between 2 and 2.3 (see Refs. 21 and 38). Most surfaces have a roll-off region for  $q < q_r$ , where  $C(q)$  is approximately constant. In calculating the rubber friction we include all the roughness components with the wavenumber  $q_0 < q < q_1$ . Here  $q_0 = 2\pi/L$ , where  $L$  is the linear size of the rubber block in the sliding direction. If  $q_0 < q_r$ , as is usually the case, the contact area and the viscoelastic contribution to the friction are nearly independent of  $q_0$ . We define the magnification  $\zeta = q/q_0$ . When we study the interface at the magnification  $\zeta$ , we do not observe roughness components with a wavenumber  $q > q_0\zeta$ , and physical quantities observed at this magnification will therefore depend on the magnification.

We note that when calculating the viscoelastic contribution to rubber friction (and the contact area), it is necessary to introduce a large wavenumber cutoff  $q_1 = 2\pi/\lambda_1$ , where  $\lambda_1$  is the shortest surface roughness wavelength included in the calculation of the contact mechanics. For smooth surfaces  $\lambda_1$  may be of the order of atomic distances, or the average distance between cross-links, i.e.,  $q_1 \approx 10^9 - 10^{10} \text{ m}^{-1}$ . For very rough surfaces, such as road surfaces, the cutoff may be related to the onset of rubber bond-breaking and wear processes, which appear in the contact regions at high enough magnifications as a result of large stresses and high temperatures. For road surfaces this typically gives the cutoff  $q_1 \sim 10^6 - 10^7 \text{ m}^{-1}$ . For rubber sliding on ice, we instead believe that  $q_1$  is determined by the plastic yield stress of ice, or at a high enough sliding speed by frictional melting which effectively removes the roughness below some characteristic length scale  $\sim 1/q_1$ .

The rubber sample was characterized by DMA (Dynamic Mechanical Analysis) for frequency and the temperature sweeps as in Ref. 37. The device was a TA-Instrument DMA Q800; the measured frequency range was 0.25 Hz–25 Hz and the temperature range  $-75$  to  $120$  °C. The data are shown in Fig. 14.

In the calculations of the viscoelastic contribution to the friction and the area of contact, we take into account the non-linear effects either by scaling the low strain modulus with the relevant strain-sweep factor  $E(\epsilon)/E(0)$  (where  $\epsilon$  is the

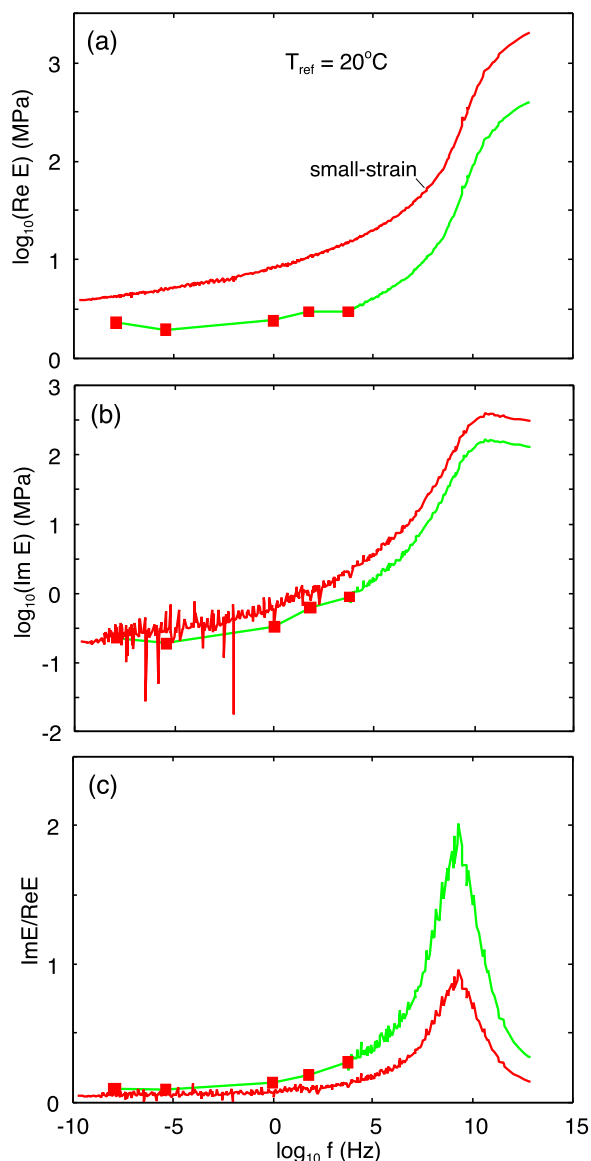


FIG. 14. The real part  $\text{Re}E$  (a) and the imaginary part  $\text{Im}E$  (b) of the viscoelastic modulus as a function of the frequency ( $\log_{10}$ - $\log_{10}$  scale). (c) The ratio  $\text{Im}E/\text{Re}E$  as a function of the logarithm of the frequency. The red lines are the linear response results for a strain amplitude of 0.04%. The red squares are the effective modulus of a strain amplitude of  $\sim 70\%$ . The green lines are the fit (and extrapolation) curves used in the calculations.

strain), or by using the green curve in Fig. 14 obtained for a typical strain value expected in the asperity contact regions (typical strain of order  $\sim 100\%$ ). Both procedures give very similar results.

The extrapolation of the effective modulus to high frequencies (green fit-lines in Fig. 14) is very uncertain since the exact non-linear viscoelastic properties of filled rubber in the high frequency region is not known. In the DMA experiments, fracture of the sample will take place at large strain and low temperature, which in the context of rubber friction would correspond to large wear. However, we believe the way we extrapolate the effective viscoelastic modulus may not be so important in most practical cases where frictional heating shifts the effective viscoelastic mastercurve to higher frequencies. Still, there is need for other better ways to study

the rubber viscoelastic properties for large strain and high frequencies.

- <sup>1</sup>WHO, *Global Status Report on Road Safety 2013: Supporting a Decade of Action* (World Health Organization, Geneva, Switzerland, 2013).
- <sup>2</sup>W. R. Chang and T. K. Courtney, *Measuring Slipperiness: Human Locomotion and Surface Factors* (Taylor & Francis, 2003).
- <sup>3</sup>M. Faraday, "Note on regelation," *Proc. R. Soc. London* **10**, 440–450 (1859).
- <sup>4</sup>R. Rosenberg, "Why is ice slippery?," *Phys. Today* **58**(12), 50–55 (2005).
- <sup>5</sup>J. R. Blackford, G. Skouvaklis, M. Purser, and V. Koutsos, "Friction on ice: Stick and slip," *Faraday Discuss.* **156**, 243–254 (2012).
- <sup>6</sup>F. P. Bowden and T. Hughes, "The mechanism of sliding on ice and snow," *Proc. R. Soc. A* **172**, 280–298 (1939).
- <sup>7</sup>B. N. J. Persson, "Theory of rubber friction and contact mechanics," *J. Chem. Phys.* **115**, 3840–3861 (2001).
- <sup>8</sup>M. Klüppel and G. Heinrich, "Rubber friction on self-affine road tracks," *Rubber Chem. Technol.* **73**(4), 578–606 (2000).
- <sup>9</sup>K. Grosch, "The relation between the friction and visco-elastic properties of rubber," *Proc. R. Soc. A* **274**, 21–39 (1963).
- <sup>10</sup>M. Rantonen, A. J. Tuononen, and P. Sainio, *Int. J. Veh. Syst. Modell. Test* **7**, 194 (2012).
- <sup>11</sup>A. Kriston, N. A. Isitman, T. Fülöp, and A. J. Tuononen, "Structural evolution and wear of ice surface during rubber-ice contact," *Tribol. Int.* **93**, 257–268 (2016).
- <sup>12</sup>Lahayne *et al.*, "Rubber friction on ice: Experiments and modeling," *Tribol. Lett.* **62**(17) 1–19 (2016).
- <sup>13</sup>P. Barnes, D. Tabor, and J. Walker, "The friction and creep of polycrystalline ice," *Proc. R. Soc. London, Ser. A* **324**(1557), 127–155 (1971).
- <sup>14</sup>T. Huemer, W. Liu, J. Eberhardsteiner, and H. Mang, "A 3D finite element formulation describing the frictional behaviour of rubber on ice and concrete surfaces," *Eng. Comput.* **18**(3/4), 417–436 (2001).
- <sup>15</sup>G. Sazaki, S. Zepeda, S. Nakatsubo, M. Yokomine, and Y. Furukawa, "Quasi-liquid layers on ice crystal surfaces are made up of two different phases," *Proc. Natl. Acad. Sci. U. S. A.* **109**(4), 1052–1055 (2012).
- <sup>16</sup>Pittenger *et al.*, "Premelting at ice-solid interfaces studied via velocity-dependent indentation with force microscope tips," *Phys. Rev. B* **63**, 134102 (2001).
- <sup>17</sup>Y. Li and G. A. Somorjai, "Surface premelting of ice," *J. Phys. Chem. C* **111**(27), 9631–9637 (2007).
- <sup>18</sup>D. Higgins, B. Marmo, C. Jeffree, V. Koutsos, and J. Blackford, "Morphology of ice wear from rubber-ice friction tests and its dependence on temperature and sliding velocity," *Wear* **265**(5-6), 634–644 (2008).
- <sup>19</sup>Engemann *et al.*, "Interfacial melting of ice in contact with  $\text{SiO}_2$ ," *Phys. Rev. Lett.* **92**, 205701-1 (2004).
- <sup>20</sup>T. Fülöp and A. J. Tuononen, "Evolution of ice surface under a sliding rubber block," *Wear* **307**, 52–59 (2013).
- <sup>21</sup>B. N. J. Persson, O. Albohr, U. Tartaglino, A. I. Volokitin, and E. Tosatti, "On the nature of surface roughness with application to contact mechanics, sealing, rubber friction and adhesion," *J. Phys.: Condens. Matter* **17**, R1–R62 (2004).
- <sup>22</sup>B. N. J. Persson, "Fluid dynamics at the interface between contacting elastic solids with randomly rough surfaces," *J. Phys.: Condens. Matter* **22**, 265004 (2010).
- <sup>23</sup>A. Kriston, T. Fülöp, N. A. Isitman, O. Kotecký, and A. J. Tuononen, "A novel method for contact analysis of rubber and various surfaces using micro-computerized-tomography," *Polym. Test.* **53**, 132–142 (2016).
- <sup>24</sup>M. Scaraggi and B. N. J. Persson, "Friction and universal contact area law for randomly rough viscoelastic contacts," *J. Phys.: Condens. Matter* **27**, 105102 (2015).
- <sup>25</sup>L. Bäurle, "Sliding friction of polyethylene on snow and ice," Doctoral dissertation (ETH Zurich, 2006).
- <sup>26</sup>P. Oksanen and J. Keinonen, "Mechanism of friction of ice," *Wear* **78**, 315–324 (1982).
- <sup>27</sup>C. Klapproth, T. M. Kessel, K. Wiese, and B. Wies, "An advanced viscous model for rubber-ice-friction," *Tribol. Int.* **99**, 169–181 (2016).
- <sup>28</sup>A. Schallamach, "Theory of dynamic rubber friction," *Wear* **6**, 375–382 (1963).
- <sup>29</sup>B. N. J. Persson, "Ice friction: Role of non-uniform frictional heating and ice premelting," *J. Chem. Phys.* **143**, 224701 (2015).

- <sup>30</sup>G. Fortunato, V. Ciaravola, A. Furno, B. Lorenz, and B. N. J. Persson, "General theory of frictional heating with application to rubber friction," *J. Phys.: Condens. Matter* **27**(17), 175008 (2015).
- <sup>31</sup>B. Lishman, P. R. Sammonds, and D. L. Feltham, "Critical slip and time dependence in sea ice friction," *Cold Reg. Sci. Technol.* **90-91**, 9–13 (2013).
- <sup>32</sup>E. M. Schulson and A. L. Fortt, "Static strengthening of frictional surfaces of ice," *Acta Mater.* **61**, 1616–1623 (2013).
- <sup>33</sup>J. M. Isomaa, A. J. Tuononen, and S. Bossuyt, "Onset of frictional sliding in rubber ice contact," *Cold Reg. Sci. Technol.* **115**, 1–8 (2015).
- <sup>34</sup>E. M. Schulson and A. L. Fortt, "Friction of ice on ice," *J. Geophys. Res.: Solid Earth* **117**, 1–18, doi:10.1029/2012JB009219 (2012).
- <sup>35</sup>A. J. Tuononen, "Onset of frictional sliding of rubber–glass contact under dry and lubricated conditions," *Sci. Rep.* **6**, 27951 (2016).
- <sup>36</sup>Y. Bar-Sinai, R. Spatschek, E. A. Brener, and E. Bouchbinder, "Velocity-strengthening friction significantly affects interfacial dynamics, strength and dissipation," *Sci. Rep.* **5**, 7841 (2015).
- <sup>37</sup>B. Lorenz and B. N. J. Persson, "Master curve of viscoelastic solid: Using causality to determine the optimal shifting procedure, and to test the accuracy of measured data," *Polymer* **55**, 565–571 (2014).
- <sup>38</sup>B. N. J. Persson, "On the fractal dimension of rough surfaces," *Tribol. Lett.* **54**(1), 99–106 (2014).
- <sup>39</sup>B. N. J. Persson, "Rubber friction: Role of the flash temperature," *J. Phys.: Condens. Matter* **18**, 7789–7823 (2006).